

# Asymmetric Excitatory Synaptic Dynamics Underlie Interaural Time Difference Processing in the Auditory System

Pablo E. Jercog<sup>1,2</sup>, Gytis Svirskis<sup>2</sup>, Vibhakar C. Kotak<sup>2</sup>, Dan H. Sanes<sup>2,3</sup>, John Rinzel<sup>2,4\*</sup>

**1** Physics Department, New York University, New York, New York, United States of America, **2** Center for Neural Science, New York University, New York, New York, United States of America, **3** Department of Biology, New York University, New York, New York, United States of America, **4** Courant Institute of Mathematical Science, New York University, New York, New York, United States of America

## Abstract

Low-frequency sound localization depends on the neural computation of interaural time differences (ITD) and relies on neurons in the auditory brain stem that integrate synaptic inputs delivered by the ipsi- and contralateral auditory pathways that start at the two ears. The first auditory neurons that respond selectively to ITD are found in the medial superior olivary nucleus (MSO). We identified a new mechanism for ITD coding using a brain slice preparation that preserves the binaural inputs to the MSO. There was an internal latency difference for the two excitatory pathways that would, if left uncompensated, position the ITD response function too far outside the physiological range to be useful for estimating ITD. We demonstrate, and support using a biophysically based computational model, that a bilateral asymmetry in excitatory post-synaptic potential (EPSP) slopes provides a robust compensatory delay mechanism due to differential activation of low threshold potassium conductance on these inputs and permits MSO neurons to encode physiological ITDs. We suggest, more generally, that the dependence of spike probability on rate of depolarization, as in these auditory neurons, provides a mechanism for temporal order discrimination between EPSPs.

**Citation:** Jercog PE, Svirskis G, Kotak VC, Sanes DH, Rinzel J (2010) Asymmetric Excitatory Synaptic Dynamics Underlie Interaural Time Difference Processing in the Auditory System. *PLoS Biol* 8(6): e1000406. doi:10.1371/journal.pbio.1000406

**Academic Editor:** Jonathan Z. Simon, University of Maryland, United States of America

**Received:** December 28, 2009; **Accepted:** May 18, 2010; **Published:** June 29, 2010

**Copyright:** © 2010 Jercog et al. This is an open-access article distributed under the terms of the Creative Commons Attribution License, which permits unrestricted use, distribution, and reproduction in any medium, provided the original author and source are credited.

**Funding:** This work is supported by National Institutes of Health (NIH) grants DC008543 and MH62595 to PEJ, GS, and JR and also NIH grant DC006864 to DHS and VCK. The funders had no role in study design, data collection and analysis, decision to publish, or preparation of the manuscript.

**Competing Interests:** The authors have declared that no competing interests exist.

**Abbreviations:** CC, current clamp; EPSPs, excitatory postsynaptic conductances; ITDs, interaural time differences; LNTB, lateral nucleus of the trapezoid body; MNTB, medial nucleus of the trapezoid body; MSO, medial superior olivary neurons; PSCs, postsynaptic currents; PSPs, postsynaptic potentials; SN, strychnine; VC, voltage clamp; VCN, ventral cochlear nucleus

\* E-mail: rinzel@cns.nyu.edu

## Introduction

In order to localize acoustic objects along the horizontal plane, the nervous system is able to distinguish microsecond differences in the arrival time of sound at the two ears, referred to as interaural time differences (ITDs). Low sound frequencies are the most useful signals for detecting ITDs, and animals with good sensitivity below 1,500 Hz tend to perform best at this perception [1]. In mammals this computation is first performed by medial superior olivary neurons (MSO) in the auditory brain stem. Each MSO neuron receives two sets of excitatory inputs on its bipolar dendrites, with each set activated by one ear. When both excitatory pathways are activated within a narrow time window, the MSO neuron detects the coincident excitatory synaptic inputs and fires action potentials. When the pathways are activated asynchronously, the MSO neurons do not respond. Thus, an ITD response function is the representation of the variation of MSO discharge rate with the relative delay of the two inputs and, therefore, the position of a sound along the horizontal plane [2].

One influential theory holds that ITD encoding is based on an arrangement of axonal delay lines [3]. In this model, the differences in the sound's time of arrival at the two ears is transformed into a spatial map of ITD detecting neurons,

sometimes referred to as a “place” code. Thus, an MSO neuron would discharge maximally when a specific ITD is exactly compensated by an internal delay that arises as a consequence of differences in the length of axons that are driven by the two ears. In fact, evidence for this mechanism has been found in birds and mammals [4–8]. However, since the discharge rate of many MSO neurons increases over the physiological range of ITDs [9–12], this information could also be used to encode the azimuthal position, sometimes referred to as the “slope” code [13]. Additionally, there is evidence to suggest that inhibitory inputs to MSO play a role in tuning the response function within the physiological range of ITDs [11,14].

In previous models of ITD processing, the propagation time between the ipsi- and contralateral ears to the MSO neurons is implicitly assumed to be equal (excluding Jeffress's internal delay lines). However, MSO neurons are positioned to one side of the brainstem, and the ipsilateral pathway is expected to be shorter than the contralateral. For example, one study has shown in vivo that many superior olivary neurons display longer latencies for the contralateral pathway [15]. Thus, any mechanism that relies on temporal precision must take this into account. We have tested this premise using a novel in vitro preparation that preserves each pathway. Our results support a new mechanistic explanation for

## Author Summary

Animals can locate the source of a sound by detecting microsecond differences in the arrival time of sound at the two ears. Neurons encoding these interaural time differences (ITDs) receive an excitatory synaptic input from each ear. They can perform a microsecond computation with excitatory synapses that have millisecond time scale because they are extremely sensitive to the input's "rise time," the time taken to reach the peak of the synaptic input. Current theories assume that the biophysical properties of the two inputs are identical. We challenge this assumption by showing that the rise times of excitatory synaptic potentials driven by the ipsilateral ear are faster than those driven by the contralateral ear. Further, we present a computational model demonstrating that this disparity in rise times, together with the neurons' sensitivity to excitation's rise time, can endow ITD-encoding with microsecond resolution in the biologically relevant range. Our analysis also resolves a timing mismatch. The difference between contralateral and ipsilateral latencies is substantially larger than the relevant ITD range. We show how the rise time disparity compensates for this mismatch. Generalizing, we suggest that phasic-firing neurons—those that respond to rapidly, but not to slowly, changing stimuli—are selective to the temporal ordering of brief inputs. In a coincidence-detection computation the neuron will respond more robustly when a faster input leads a slower one, even if the inputs are brief and have similar amplitudes.

the compensation of a longer contralateral response latency, and the positioning of the ITD response function in the physiological relevant range. The mechanism takes advantage of a difference in the dynamics of ipsi- and contralateral excitatory synaptic inputs. Using a computational model, we demonstrate that these asymmetric excitatory synaptic dynamics can significantly alter the ITD responses of MSO neurons.

## Results

Asymmetries in circuit architecture can have a significant effect on ITD processing. Specifically, the contralateral projections from ventral cochlear nucleus (VCN) to MSO are longer than those from the ipsilateral side (Figure 1A, difference in afferent lengths between ipsilateral VCN to MSO and contralateral VCN to MSO  $\approx 2.45$  mm; Paul Nakamura and Karina Cramer, personal communication). To measure this difference functionally we used a thick brain slice preparation from gerbils that preserves the afferent pathways to the superior olivary complex (Figure 1A; see Methods). Whole cell recordings were obtained from MSO neurons while activating each pathway at the same anatomical position on each side; the pathway between the stimulation point and the cochlea, which is eliminated in this preparation, is assumed to be identical for each side (Figure 1A). We first found that the response latency did, in fact, differ between the two pathways. An analysis of evoked postsynaptic potentials (PSPs) and currents (PSCs) showed that the latencies to peak of contralateral responses were on average about  $500 \mu\text{s}$  longer than those of ipsilateral responses on the same recorded neuron (Figure 1B,C; average differences in latency to peak for PSPs:  $573 \pm 62 \mu\text{s}$ ,  $n = 54$ ; for PSCs:  $589 \pm 81 \mu\text{s}$ ,  $n = 37$ , see Methods section). This difference was apparent on a cell-by-cell basis because the difference of latencies (contralateral - ipsilateral) was significantly different than zero (see gray bars in Figure 1B).

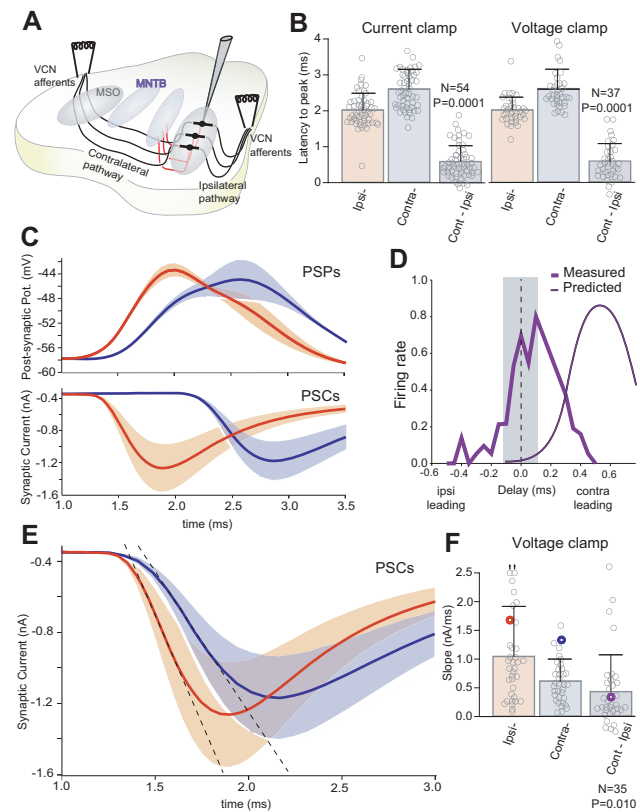


**Figure 1. Time difference processing in gerbil MSO in vitro.** (A) Schematic of thick slice preparation (500  $\mu\text{m}$ ) through the ventral auditory brain stem. Afferent projections from the ipsi- and contralateral VCN are segregated on MSO dendrites. MNTB inhibitory afferents provide contralaterally evoked inhibition to MSO neurons. It is important to recognize that the stimulating electrodes are placed at a position on the auditory pathway that has the same axonal length to the ears, respectively, on each side. (B) PSPs- and PSCs-latency to peak responses (different population sets: voltage clamp data were recorded with intracellular cesium and QX-314). Population's average and standard deviation to show the range of MSO delays. Statistical intervals of confidence were expressed using *t* test with respect to zero for the difference between ipsilateral and contralateral responses on the same neuron (right column: Cont-Ipsi). (C) Average and standard deviation of PSPs and PSCs (average of 50 trials per neuron) for two different sample neurons. The superimposed traces show that the contralateral response occurs at a longer latency. (D) ITD response function in vitro. Bilateral stimulation of VCN afferents elicits action potentials in MSO neurons through coincidence detection of the bilateral PSPs. Gerbil's physiological relevant range (gray bar). Spikes were counted at different stimulation delays to mimic physiological ITD response functions (Measured). Based on the average delay between ipsilateral and contralateral PSPs latency to peak, the ITD response function should be maximal at  $580 \mu\text{s}$  on the contra-leading side ("Predicted" curve is hypothetical, based on bilateral PSP-peak coincidence). The ITD response function peak is close to zero-delay when the bilateral PSPs are summated by the neuron, creating a paradox between the predicted and measured responses. (E) Average and standard deviation of PSCs (average of 50 trials for a sample neuron). The superimposed traces show that the ipsilateral rising slope is steeper. (F) Population data for PSC slopes. Statistical intervals of confidence were expressed using *t* test versus zero for the difference between ipsilateral and contralateral responses on the same neuron (right column: Cont-Ipsi). PSCs in (E) are marked with colored circles. Difference in PSCs is our explanation for the paradox stated in D. doi:10.1371/journal.pbio.1000406.g001

In presenting the following experiments, we refer to the in vitro inter-stimulus time difference as ITD. Thus, if threshold were to depend solely on PSP amplitude, then the measured disparity in PSP latencies would predict that the peak ITD response would occur when the contralateral PSP leads by approximately 500  $\mu\text{s}$  (Figure 1D; predicted, thin curve). This ITD value is sufficiently large that the response function would fall largely outside of the physiological range for gerbils, which is  $\pm 130 \mu\text{s}$  [16]. In contrast, we found ITD response functions in which MSO firing rate was maximal when bilateral stimuli were delivered with smaller delays of  $\approx 100 \mu\text{s}$  (Figure 1D; measured, thick curve). This finding suggests that an intrinsic integration mechanism must compensate for the longer contralateral path.

MSO neurons are exquisitely sensitive to the rate of depolarization. Therefore, in order to understand the integration of subthreshold bilateral inputs that lead to a spike, we examined the dynamics of synaptic inputs. Our starting assumption had been that synaptic properties are identical for each of the two excitatory inputs to MSO. We examined this assumption by measuring the rising PSP slopes because their time scale is within the same range as the coincidence detection window as manifested by the width of the ITD response function (i.e., 0–250  $\mu\text{s}$ ). Ipsilaterally evoked PSCs had significantly steeper rising slopes than contralateral PSCs (Figure 1E,F) (ipsilateral:  $1.04 \pm 0.15 \text{ nA/ms}$ , contralateral:  $0.62 \pm 0.06 \text{ nA/ms}$ ;  $p = 0.01$ ,  $n = 35$ ). This difference was apparent on a cell-by-cell basis because the difference of PSC slopes (contralateral - ipsilateral) was significantly different than zero (see gray bar in Figure 1F). This result was independent of stimulus amplitude in all tested neurons (see Figure S1). The differences in the slopes of the PSCs could compensate, in part, for the disparity

in delay between the two pathways. Our computational model (below) showed that even a modest asymmetry in rising slopes could shift the ITD response function from its hypothetical position (based on latencies to peak) to the observed location in the in vitro experiment (Figure 1D).

To determine how this asymmetry in excitatory synapse kinetics might compensate for the differences in path length, it was first necessary to determine the contribution of synaptic inhibition. To address this issue, we obtained ITD response functions under current clamp (CC), before and after application of a glycine receptor antagonist, strychnine (SN). As shown in Figure 2A and 2B, when synaptic inhibition was present (control), the maximal firing occurred for contralateral leading stimulation, consistent with in vivo recordings [9–12]. When synaptic inhibition was blocked (Figure 2A and 2B, SN) the maximal firing rate was close to zero ITD, also consistent with an in vivo study [11]. We calculated the ITD at which peak firing probability occurred (“best ITD”) for the population of recorded neurons (Figure 2C) and found that under control conditions the peak was at  $105 \pm 35 \mu\text{s}$  (contra-leading), while under SN conditions it was at  $-62 \pm 38 \mu\text{s}$  (ipsi-leading). Therefore, the effect of synaptic inhibition was to shift ITD tuning towards contralateral leading stimuli. Since this shift is in the wrong direction to compensate for the longer contralateral path, we next considered the role of asymmetric excitatory responses.

In the presence of inhibition (control), the ipsilaterally evoked normalized PSP slope was  $2.71 \pm 0.12 \text{ ms}^{-1}$  and the contralateral slope was  $2.49 \pm 0.10 \text{ ms}^{-1}$  (Figure 2D). When inhibition was blocked (SN), evoked EPSP slopes were significantly different between ipsi- and contralateral responses (ipsilateral:

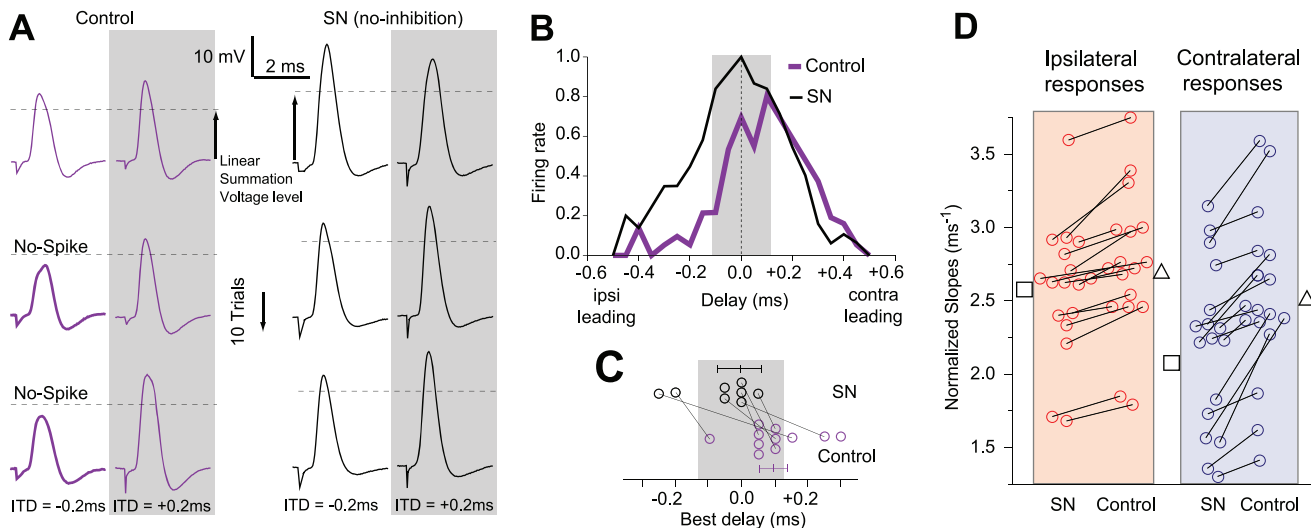


**Figure 2. Effect of asymmetric PSPs and EPSPs in setting best ITD position.** (A) Voltage time courses of somatic depolarization under bilateral stimulation at different delays (example cell, P21, T = 32°C). Each column shows three representative trials for a specific ITD value. The dashed lines show the spike identification-threshold for our experiments, and these were used to plot the ITD functions shown in (B). When glycinergic inhibition was blocked (SN), firing rate increased for ipsilateral leading ITD stimulations (compare column 1 (1 spike in 3 trials) with column 3 (3 spikes in 3 trials)). (B) ITD response function for control case and when blocking synaptic inhibition (SN) for 10 stimulation trials. Shaded area is the physiologically relevant range ( $\pm 130 \mu\text{s}$ ). (C) Best ITD response for different cells under control and with SN. Shaded area is the predicted best ITDs for control should be around 580  $\mu\text{s}$  on average. Instead our data show that best ITD responses are closer to a delay of zero. When inhibition is blocked the best ITDs shift towards ipsi-leading responses ( $N = 12$ , postnatal days 17–25; disconnected points are from experiments that were performed either in control or under SN only). (D) Increase in slope when inhibition is present. Slopes for normalized EPSP (SN, no-inhibition) are: ipsi  $2.61 \pm 0.11 \text{ ms}^{-1}$  (square), contra  $2.21 \pm 0.14 \text{ ms}^{-1}$  (triangle);  $p = 0.031$ ,  $n = 17$ . When inhibition is present (Control) PSP slopes are: ipsi  $2.71 \pm 0.12 \text{ ms}^{-1}$ , contra  $2.49 \pm 0.10 \text{ ms}^{-1}$ ;  $p = 0.064$ ,  $n = 17$ . Stronger effect of the inhibition on contralateral responses (contra-inputs difference  $0.28 \text{ ms}^{-1}$ ,  $p = 0.05$ ,  $n = 17$ ; ipsi-inputs difference  $0.10 \text{ ms}^{-1}$ ,  $p = 0.05$ ,  $n = 17$ ). Bilateral EPSPs are even more asymmetric than the PSPs, suggesting a possible explanation for why best ITDs are more shifted to the ipsi-leading side under SN (see below model results, Figure 5). doi:10.1371/journal.pbio.1000406.g002

$2.61 \pm 0.11 \text{ ms}^{-1}$ ; contralateral:  $2.21 \pm 0.14 \text{ ms}^{-1}$ , see Figure 2D and also Figure S2). Blockade of glycinergic inhibition increases the differences in the PSP slopes. More specifically, inhibition always increases the slope (Figure 2D, from squares to triangles), but more so for the contralateral responses (Figure 2D, right column). Such steepening occurs for either fast or slow inhibitory synaptic conductance transients (see Figure S3 for theoretical support). In the fast case (Figure S3, left), the decaying brief IPSC coincides with rising EPSC and the summed current therefore rises faster than the EPSC alone. The effect is stronger on contralateral inputs because the IPSC will more fully decay during the EPSC rise. In the slow case, the IPSC transiently reduces the effective time constant, accelerating the rise although less dramatically than does a fast IPSC (Figure S3, right). The effect is stronger for contralateral inputs partly because integration of slower inputs is affected more by time constant changes (leakage matters in addition to capacitive integration). Another major contributing factor related to active currents is explained below with our model. Thus, we confirmed that synaptic inhibition reduced the effect of shifting the ITD response function towards zero ITD, and leads us to suggest that the compensation arises from the excitatory asymmetry described above (Figure 1).

How can such a small asymmetry in EPSP slope influence ITD sensitivity in MSO neurons? We addressed this question by using a computational MSO neuron model that was driven by bilateral trains of excitatory and inhibitory inputs temporally modulated with a periodic function representing VCN responses to pure tone stimuli. Each cycle's composite input was generated from many small excitatory postsynaptic conductances (EPSCs) with statistics that depended on VCN afferent activity that varied with sound frequency and amplitude (see Methods; [17,18]). Figure 3 shows a simplified version of the simulated MSO inputs to illustrate the variability of the composite EPSCs and integrated EPSPs due only to the jitter on the mini-EPSCs time release. Here, we exclude firing rate modulation throughout the sinusoidal input's cycles, although it is employed in the detailed model used for the simulated ITD functions. Using only differences in vector strength of the simulated inputs from the VCN arriving to each dendrite of the MSO neuron model we modeled differences in rising slope of the bilateral EPSPs (Notice: without delaying the composite EPSP peak, see triangles in Figure 3 for EPSC peaks). These differences led to shifts in the ITD response function that are large enough to compensate for the longer contralateral input pathway. For a given EPSC input, the evoked EPSPs and spike threshold will be determined by the active currents. In MSO and other auditory processing centers, a *low threshold potassium current* ( $I_{KLT}$ ) exerts control on spike threshold [19–21]. This fast  $I_{KLT}$  imposes a filtering effect on the synaptic inputs allowing only steep EPSC slopes to evoke an action potential [22,23]. Therefore, steeper EPSCs are more likely to trigger spikes, even when shallower EPSCs may have greater amplitude, as is shown in our simulations.

When bilateral subthreshold inputs arrive at an MSO neuron, there is a higher probability of eliciting a spike when the steeper EPSC arrives first. Figure 4A shows how a pair of EPSCs, one fast and one slow, can produce a very different outcome, depending on their order of arrival. When a faster input arrives first this will enable spike generation (Figure 4A and 4B, left side). When a slower input arrives earlier it leads to a slower rising EPSP that recruits more  $I_{KLT}$  conductance, which hinders spike generation even though a faster EPSC arrives subsequently (Figure 4A and 4B, right side).

To show the essence of the ITD response function shift due to the asymmetry in the kinetics of the excitatory inputs we delivered

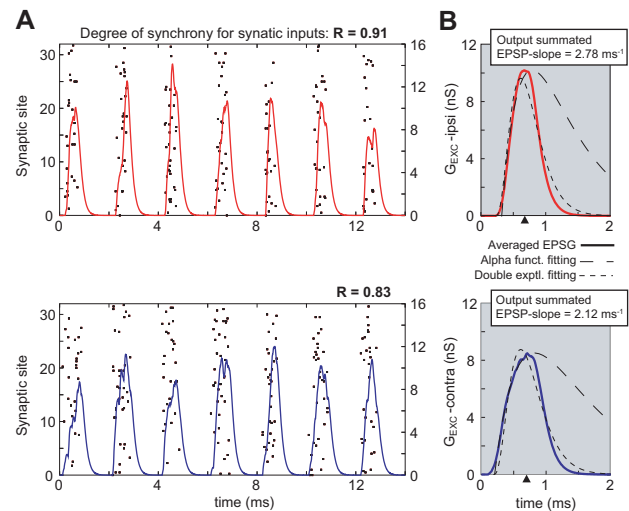


**Figure 3. Example of composite EPSCs for an input train (500 Hz) using an idealized auditory nerve fiber model (sinusoidally modulated Poisson rate for mini-EPSC times).** It is less realistic than Carney's model (1993)[18] that we used for Figures 4 and 5. (A) Raster plots with event times for ipsilateral excitatory inputs (red) and contralateral excitatory inputs (blue). Superposition of composite EPSCs for the two cases. Mini-EPSCs are alpha functions with time constant of 0.1 ms (see Methods). The difference in vector strength (degree of synchrony) between the events dictates the shape of the composite EPSCs. (B) Average over 25 cycles of composite EPSCs for the two different input cases. In the two cases a function (dashed) was fitted to the average EPSC. Alpha function is the simplest description of EPSCs (long dashes); it fits the rising phase but not the falling phase. For our summed EPSCs a more complicated function (see below) matches better the envelope or composite EPSC (in the case of excitation). EPSCs integrated through our MSO neuron model give EPSPs rising slopes that are steeper when vector strength is larger (normalized ipsi-EPSP's slope  $2.78 \text{ ms}^{-1}$ , contra-EPSP's slope  $2.12 \text{ ms}^{-1}$ ). Composite EPSCs in (B) are fitted by functional form that is proportional to  $(1 - \exp(-(t-t_0)/\tau_{\text{rise}})) \cdot 3 \cdot (\exp(-(t-t_0)/\tau_{\text{decay}}))$ . Ipsilateral inputs (red):  $\tau_{\text{rise}} = 2.5$ ,  $\tau_{\text{decay}} = 0.14$ . Contralateral inputs (blue):  $\tau_{\text{rise}} = 2.8$ ,  $\tau_{\text{decay}} = 0.18$ . For the alpha functions fits, for ipsilateral inputs (red):  $\tau = 0.48$ ; for contralateral inputs (blue):  $\tau = 0.69$ . All  $\tau$  values in ms. Note: the position of the peak of the summed EPSP does not depend on vector strength (see dark triangles in B). doi:10.1371/journal.pbio.1000406.g003

inputs to the model with different vector strength (Figure 3) and calculated their probability to evoke spikes for different input delays (ITD response function, Figure 4C,D). If the contralateral composite EPSP was slower-rising, the bilateral combined EPSP had different rising dynamics when the ipsilateral inputs led than when the contralateral inputs led (Figure 4C, EPSPs schematics). Consistent with previous findings [21,24–26], the shallower-leading combined EPSP was associated with a lower probability of firing. Therefore, the ITD function shifted towards the ipsilateral leading side (Figure 4C). The asymmetry in firing rate probability caused by an asymmetry in inputs' rising slopes is due to the voltage-dependence of  $I_{KLT}$  conductance. We explain this (Figure 4D) by showing that with the same set of bilateral asymmetric EPSPs that generate a shift of  $\sim 400 \mu\text{s}$  (Figure 4D, thick black curve), the shift of the ITD's response function disappears (Figure 4D, brown curve) if we fix the  $I_{KLT}$  conductance at its resting value, in order to maintain the neuron model's time constant and input resistance intact.

We next asked whether the asymmetry in the excitatory inputs could compensate for an intrinsic input delay of  $\approx 500 \mu\text{s}$  as measured in our in vitro preparation. The simulations showed that

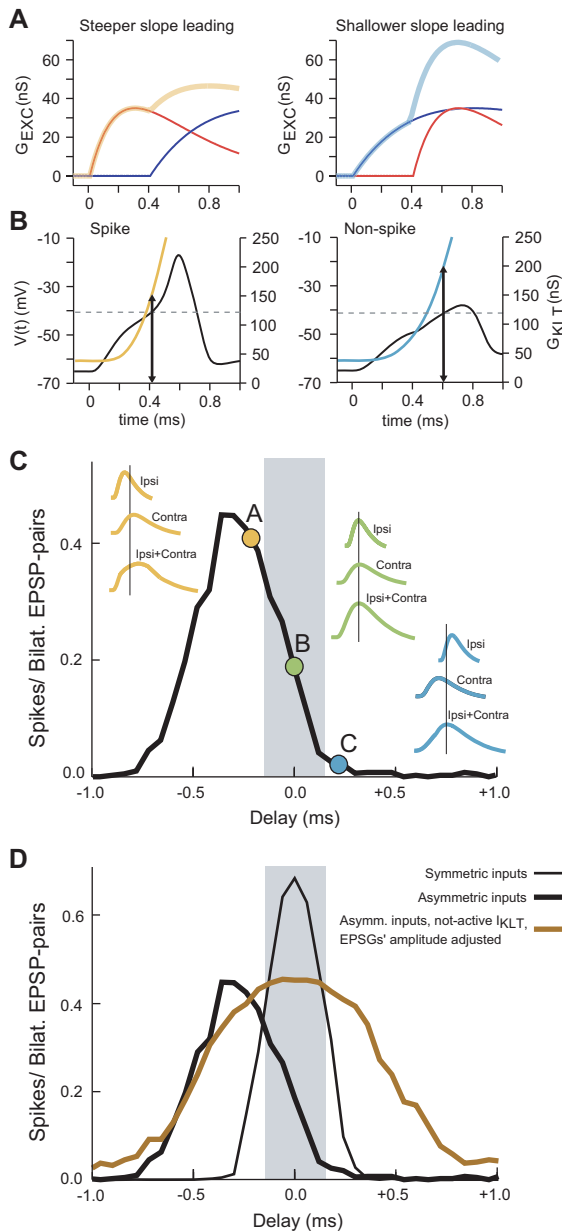


**Figure 4. The differential dependence of spike probability on EPSP's slope disappears when  $I_{KLT}$  is disabled.** (A) Pairings of EPSPs with different time constants and different temporal order. Left: steep EPSP (red curve) arrives earlier than shallow EPSP (blue curve). The summated EPSP pair (steeper then shallower, ipsi then contra) leads to a spike. Right: same EPSPs with reverse order but same time difference does not generate a spike. Inputs' delays different than zero in which steeper EPSP is arriving earlier will generate more spikes than the inputs' delays with the opposite order of arrival time. (B) Voltage time courses (black curves) for the case of spike and non-spike illustrated in (A).  $G_{KLT}$  (orange and light blue curves) corresponding to the same two temporal ordering cases. Amount of  $G_{KLT}$  recruited (arrows) for the same voltage amplitude in the two time order cases. The deflection in voltage prior to spike generation is indicated by a dashed line. Notice: the amount of  $G_{KLT}$  is higher in the case of the shallower EPSP leading; this yields the same proportional increase for  $I_{KLT}$  since driving force is the same in both cases. For a given pair of EPSPs, the steeper EPSP arriving first recruits less  $G_{KLT}$  and therefore decreases spike threshold level. (C) ITD function shifting due to asymmetric EPSPs. Simulation for ITD detection with asymmetric EPSPs using Carney's (1993)[18] synaptic input model (bilateral EPSP trains at 500 Hz). Colored time courses: schematics of the combination of EPSP-

pairs (without spike; vertical lines are to identify relative time delays), three cases: ipsi-leading (steeper then shallower, A), perfect coincidence ITD=0 (B), and contra-leading (C). Pairs in (A), (B), and (C) cases have different rising slope. Maximum firing rate is generated for the steepest rising EPSP-pair (steep ipsi-EPSP leading) as explained in (A). (D) Differential dependence on EPSP's slope disappears when  $I_{KLT}$  is disabled. Thin black curve: ITD function for bilaterally symmetric inputs (vector strength,  $R=0.9$ ). Thick black curve: ITD function for asymmetric inputs ( $R_{IPSI}=0.95$ ,  $R_{CONTRA}=0.63$ ), same curve as in (C). Thick brown curve:  $G_{KLT}$  is frozen at its rest value preserving the model's passive properties ( $I_{KLT}$  behaves as a passive current). For comparison, EPSPs are adjusted to give the same spike probability as in the previous case. doi:10.1371/journal.pbio.1000406.g004

the integration of hypothetical symmetric EPSPs led to an ITD response function that was shifted to the contralateral leading side due to the intrinsic contralateral axonal delay (Figure 5, thin black curve). When asymmetric EPSPs were introduced in the model to generate EPSP slopes similar to those found in our experiments, the ITD function shifted towards the ipsilateral-leading direction due to the favorable response when a steep EPSP occurs first (Figure 5, thick black curve).

Our experimental data were consistent with this theoretical explanation: most of the neurons displayed this asymmetry in excitatory inputs. Thus, when we subtracted contralateral slope from ipsilateral slope for each individual neuron, the average difference was  $0.69 \pm 0.18$  nA/ms for EPSCs and  $0.40 \pm 0.12$  ms<sup>-1</sup> for normalized EPSPs. Inclusion of synaptic inhibition made the simulated EPSPs less asymmetric. The hyperpolarization from inhibition transiently reduced  $I_{KLT}$ . The reduction of this conductance would no longer favor spike generation when fast EPSPs are followed by slow EPSPs. The ITD response function was reduced on the ipsilateral-leading side, giving the appearance

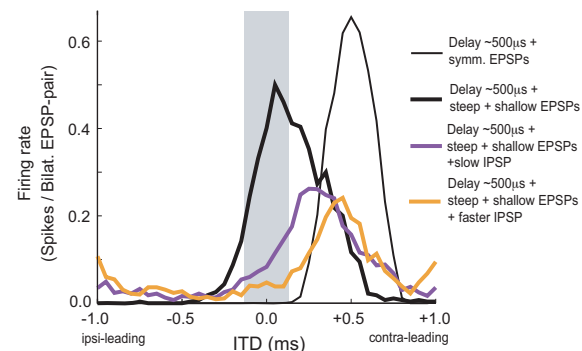


**Figure 5. Model prediction of ITD response function using experimental data.**  $R$  is the vector strength of the monolateral presynaptic input. Bilateral input trains of 500 Hz. Thin black curve: simulated ITD function if EPSPs are symmetric. Longer contralateral delay of 500  $\mu$ s, as our experimental data show. If the pre-synaptic afferents are symmetric, each with  $R=0.90$ , the rising phase (only) of the summated EPSPs was fit by an alpha-function with  $\tau_{exc}=0.14$  ms (EPSP-slope =  $2.75$  ms<sup>-1</sup>). Thick black curve: same contralateral delay as the previous case but with asymmetric excitatory inputs. Contra- is shallower than ipsi-, slope-ipsi-EPSP =  $3.1$  ms<sup>-1</sup> ( $R=0.93$ , mini-EPSP- $\tau_{exc}=0.1$  ms), slope-contra-EPSP =  $1.6$  ms<sup>-1</sup> ( $R=0.60$ , EPSP- $\tau_{exc}=0.1$  ms); for EPSP shapes see also Figure S4. Violet curve: adding contralateral inhibition preceding excitation by 0.2 ms shifts ITD function towards contralateral leading inputs; slow IPSPs (IPSP-slope =  $0.6$  ms<sup>-1</sup> ( $R=0.5$ , IPSP- $\tau_{inh}=0.4$  ms)). Orange curve: faster IPSP than previous case creates larger shift (IPSP-slope =  $0.95$  ms<sup>-1</sup> ( $R=0.7$ , IPSP- $\tau_{inh}=0.4$  ms)). doi:10.1371/journal.pbio.1000406.g005

of a shift towards the contralateral-leading side (Figure 5, orange and violet curves), as observed experimentally *in vitro* (Figure 2B) and as reported previously *in vivo* [11,14].

## Discussion

Our experimental and computational findings identified key biophysical factors that, together, position the ITD response function in the biologically relevant range. We first confirmed the presence of an internal delay of the longer contralateral pathway (Figure 1B). In itself, this would cause MSO neurons to fire mostly to ITDs with stimuli having large contralateral leading stimuli that are outside the physiological range. Our experimental and computational results suggest a novel excitatory synaptic mechanism that could compensate for the disparity in path length. An asymmetry in the slopes of EPSPs (Figure 2D) can bias the ITD coding in favor of the ipsilateral-leading inputs (Figures 4 and 5), and this repositions the ITD function within the physiological range, as found *in vivo* [9–12].

The presence of a fixed internal latency difference will affect all models of ITD processing. Jeffress [3] assumed tacitly that the two paths were equal in length except for the small differences along one spatial axis of the encoding nucleus. Others have suggested that the shorter path length from the ipsilateral ear is compensated by an additional span of axon (e.g., see schematic in [2]), or a difference in myelination between the two pathways [27]. If the difference in path length to MSO for the gerbil is  $\approx 2.45$  mm (Paul Nakamura and Karina Cramer, personal communication), then our electrophysiological measurements of response latency difference of  $500 \mu\text{s}$  would yield a propagation speed of  $4.9$  m/s. Thus, it appears that there is an internal latency difference to gerbil MSO that is not compensated for by an axonal property. It is this functional characteristic that must be addressed if MSO neurons are to encode ITDs in the physiological range ( $\pm 130 \mu\text{s}$ ; [16]).

Our electrophysiological measurements indicate that the rising PSP slope is larger for the ipsilateral input to MSO neurons on a cell-by-cell basis (Figures 1 and 2). The functional implications for this finding are illustrated in a computational model which demonstrates that this property can compensate for the aforementioned difference in path length (Figure 5). The general principle, which is that the rising slope of an EPSP determines the probability of firing, is consistent with findings from other systems [21,25,26,28]. Here, we have adapted this principle to resolve the general problem of compensating for different input latencies due to path length.

How might the EPSP asymmetry arise? In the model we allowed for more jitter in the arrival times of identically shaped unitary (minimal) EPSPs on the contralateral side, which slowed the rise of the composite EPSPs. This idealization, for demonstrating plausibility in the context of our point neuron model, could be elaborated and explored in a neuron model that has bilateral dendrites with cable properties [29]. Many alternative mechanisms are also possible. Bilateral differences in dendritic morphology or the dendritic positioning of excitatory terminals could also lead to an asymmetry in the rising slope of composite EPSPs [30,31]. Although longer electrical distances would promote broadening of composite EPSPs in a passive dendrite,  $I_{\text{KLT}}$  in the dendrites can reduce the effect by shortening the tail of EPSPs as they propagate toward the soma in MSO neurons and cable models [32]. Alternatively, the distribution of active currents could modulate the dendritic integration of synaptic inputs. For example, dendritic sodium channels are able to selectively boost EPSPs on one dendrite, and this would modify their rising slope (cortex: [33]).

It is important to consider the *in vivo* time scale of inhibition and excitation because it will determine the temporal integration window and the extent to which ITD curves will be affected by the mechanisms described above. It is possible that the time scales *in vivo* are faster than in the brain slice because a cell is in a high conductance state (e.g., many more active inputs as compared to brain slice). In addition, the degree of afferent synchrony could have been unnaturally high in our preparation because the stimulus simultaneously recruits all VCN afferents to MSO. However, the model demonstrated that the effect of slope is robust when implemented with vector strength values that have been reported *in vivo* (Figure 3; using model from [18]). Since we also showed that synaptic inhibition somewhat counteracts the shifting effect of the asymmetric excitation, it is important to consider its kinetics. The time scale for inhibition has only been studied *in vitro*, and even the fastest IPSPs have either been recorded from animals between 12 to 25 postnatal days [34], or at room temperature [35]. Interestingly, we found that while the magnitude of the inhibitory effect depends on IPSP time scale, it is likely to play an important role in ITD coding no matter what the actual time scale value turns out to be (Figure 5; Figure S3).

The faster rising EPSPs that were elicited by ipsilateral afferents could overcome the penalizing effect of a rapidly activating outward current like  $I_{\text{KLT}}$  (Figure 4B). Many previous reports have demonstrated a robust effect of  $I_{\text{KLT}}$  on the integration time of EPSPs [19,20,28]. In this study, we applied this property to anatomically independent bilateral inputs and demonstrated computationally that  $I_{\text{KLT}}$  influenced the ITD function.

Together, our findings lead us to propose a general principle. Passive neuronal integration to a threshold would not distinguish the temporal ordering in inputs that may have different rising slopes. Subthreshold dynamic negative feedback such as  $I_{\text{KLT}}$  (comparably as fast as integration) will bias the integration. Firing will be favored when the steeper-rising input occurs first. Inhibition, by deactivating the negative feedback, can reduce the bias. The competition between these two effects in the MSO, leads to a positioning of the ITD response function with its slope in the physiological range, as seen *in vivo* [11]. Thus, the synaptic property compensates for the intrinsic latency disparity. Time-difference encoding could exploit these mechanisms in this extremely short window of integration time ( $130 \mu\text{s}$ ) or, more generally, in other windows where the biophysical components and time scales are appropriately matched. Generalizing, we propose a novel neuronal mechanism for temporal order selectivity. Subthreshold dynamic negative feedback can increase a neuron's firing probability to segregated subthreshold inputs when faster ones precede slower ones, even if the slower one is of similar or larger amplitude.

## Methods

### Experiments

All protocols were reviewed and approved by New York University Institutional Animal Care and Use Committee. Postnatal day (P) 17–25 gerbils (Charles River) were used to generate thick ( $450\text{--}500 \mu\text{m}$ ) horizontal slices ( $N=91$ ) from the ventral auditory brainstem. Each slice contained the MSO nucleus, the medial nucleus of the trapezoid body (MNTB), and the lateral nucleus of the trapezoid body (LNTB). Animals were deeply anesthetized (chloral hydrate,  $400$  mg/kg), perfused intracardially with artificial cerebrospinal fluid (ACSF:  $123$  mM NaCl,  $4$  mM KCl,  $1.2$  mM  $\text{KH}_2\text{PO}_4$ ,  $1.3$  mM  $\text{MgSO}_4$ ,  $24$  mM  $\text{NaHCO}_3$ ,  $15$  mM glucose,  $2.4$  mM  $\text{CaCl}_2$ ,  $0.2$  mM ascorbic acid;  $\text{pH}=7.35$  after bubbling with  $95\%$   $\text{O}_2/5\%$   $\text{CO}_2$ ) at  $32^\circ\text{C}$ . The

brain was then dissected free in 32°C oxygenated ACSF, and one horizontal slice was obtained with a Leica vibratome. The slice was incubated at 36°C for 20 min, and at 22°C for 1 h before being transferred to the recording chamber where oxygenated ACSF was perfused at a rate of 2 ml/min at 32°C; temperature was regulated by I&N temperature controller.

The afferents arising from both VCNs were visualized as compact bundles. Thus, ipsilateral and contralateral bundles were stimulated at the site of their origins with bipolar tungsten electrode and stimulation was delivered by two stimulus isolation units (Dagan). The distance between the MSO and the two stimulation sites was approximately 0.5 mm for the ipsilateral pathway and 1.5 mm for contralateral pathway. Whole cell current-clamp recordings were obtained mostly from medial and dorsal MSO neurons (Axoclamp2A). The recordings and stimulation were computer driven (Windows XP) through Labview software (National Instruments). The neurons were visually identified using infra-red differential interference contrast (IR-DIC) microscopy (Olympus). The internal patch solution contained (in mM) 127.5 potassium gluconate, 0.6 EGTA, 10 HEPES, 2 MgCl<sub>2</sub>, 5 KCl, 2 ATP, 10 phosphocreatinine (Tris salt), and 0.3 GTP (pH 7.2) in the case of CC protocol and (in mM) 127.5 cesium gluconate, 0.6 EGTA, 10 HEPES, 2 MgCl<sub>2</sub>, 5 KCl, 2 ATP, 5 QX-314, 10 phosphocreatinine (Tris salt), and 0.3 GTP (pH 7.2) in the case of voltage clamp (VC) protocol. In order to block synaptic inhibitory inputs, we used SN in CC experiments and SN and bicuculine to block glycinergic/gabaergic inputs in VC experiments.

EPSPs in CC and EPSCs in VC were recorded when single square pulses repeatedly (20 Hz) of 25–50 μs were delivered via the stimulating electrodes to initially evoke minimum amplitude responses, maximum amplitude subthreshold responses, and subthreshold-unilateral/suprathreshold-bilateral responses. High stimulus currents (0.5 to 10.0 mA) and short pulse durations (25–50 μs) were used to avoid the overlap of stimulus artifact with evoked responses. The data were analyzed following these basic criteria: slopes of the rising phase (20% to 80%) of the responses, for unilateral stimulations. For all the parameters that were measured for bilateral stimulations responses (i.e., peak-delay, slope), the intervals of confidence (*p* values) were computed using *t* test over the difference between ipsi- and contralateral responses on the same neuron. All data variability is expressed in standard deviation. In addition, 100 to 500 Hz stimulus trains of 10 stimuli were applied (total number of spikes per train delay were counted) to generate ITD tuning response function. A minimum of four trials were run to get a smooth ITD response function. In the case of CC data the slopes of PSPs and EPSPs were computed when bilateral responses were similar in amplitude, to avoid differential effect of active currents, and were normalized to decrease population variability due to biophysical heterogeneity among neurons.

## Simulations

We used a computational model of MSO neurons based on the parameters described by Rothman and Manis (2003)[36] for a point VCN neuron [36]. We chose a membrane time constant of 0.3 ms, similar to the one reported for MSO neurons after P20 [20]. Bilateral input trains with different delays were created by injecting currents (conductance based synaptic-like currents) such that the trains of EPSPs consisted of composite minimal EPSPs (32 or 64 minimal EPSPs were used to create a ~8 mV composite EPSP; more EPSPs were used for higher input frequencies (1.1 KHz) to generate a smooth voltage time course). Minimal EPSPs had fixed form: alpha functions with time constant  $\tau_{syn}$  of

0.1 ms for excitation and 0.4 for inhibition, scaled to have specified area and peak proportional to  $1/\tau_{syn}$ . Different minimal EPSP statistics led to different slopes and half-widths, which are summed in order to create the composite suprathreshold EPSPs (see Figure S4). These EPSPs have envelopes resembling alpha functions with time constants that ranged from 0.1 to 0.8 ms [17]. This range of (in vivo based) EPSP time constants was slightly faster than those obtained from our experiments because our recordings were made at 32°C and the simulations were performed at 37°C. The same results were obtained using values of rising EPSP slopes from our experiments at 22°C as well as the kinetics of our computational model, to eliminate any temperature effect.

The asymmetry in simulated EPSP kinetics was modeled by varying the jitter of unitary events. The amount of jitter was based on the observed variability in EPSC amplitudes, slopes, and half-widths obtained in our brain slice recordings. ITD functions were created from bilateral EPSP or PSP trains (40 cycles) at frequencies ranging from 250 to 1,100 Hz. A minimum of 10 trials (per ITD) were run to get a smooth ITD response function.

The differential equations of the model were integrated numerically using fourth-order-Runge-Kutta scheme with a time step between 1 and 0.25 μs; refining the time step did not lead to noticeable differences in the computed solutions.

In all the simulations the contralateral inhibitory input leads the contralateral excitation by 0.2 ms. This time difference was imposed between the peak of the composite IPSPs and the composite EPSPs from the contralateral input side. The result in Figure 4 showing that inhibition shifts the ITD response function towards contralateral leading side holds even for bigger delays between contralateral inhibition and excitation (unpublished data).

## Supporting Information

**Figure S1 PSP-rising-slope and -peak-delay versus PSP response amplitude for different VCN-afferents stimulation strength.** (A) Examples of individual neurons showing that asymmetry of rising slopes between bilateral inputs remains, when the response amplitude changed (top: current clamp experiment, P21; bottom: voltage clamp experiment, P23). (B) The distribution of peak latencies for PSP responses is almost flat for the range of subthreshold PSPs and PSCs (top and bottom plots, respectively, same neurons in A). (C) Summarized data for 14 experiments in current clamp and 16 in voltage clamp configuration (see Methods). Left: rate of change for slope at different amplitude responses is similar between sides, supporting the result that when PSP slopes are asymmetric between sides they will remain asymmetric through the subthreshold range. Right: rate of change of latencies is close to zero for different response amplitudes. Even though the individual monolateral response has jitter, the ITD response function is the average latency of the PSP responses and this is statistically unchanged with the amplitude of the response.

Found at: doi:10.1371/journal.pbio.1000406.s001 (0.63 MB EPS)

**Figure S2 Subthreshold evoked-PSPs stimulating the afferents of the VCN onto the MSO neurons on our thick slice preparation.** (A) In most of the neurons recorded ipsilateral responses were bigger in amplitude than the contralateral; for this reason all the data in the paper are normalized by amplitude to avoid bias on the comparison between contralateral and ipsilateral rising-phase slopes. Cells had been recorded from both olives on the same slice, keeping the stimulating electrodes on the same location to avoid possible sources of asymmetries due to the stimulation artifacts. Time courses show that PSPs are a

composition of many synaptic mini-PSPs released with a particular distribution of locations and/or timing. Dendrite morphology could play a role on the asymmetry in EPSPs' shapes. Superposition of ipsilateral and contralateral responses shows a consistent trial-to-trial difference on rising phase. (B) When inhibition is blocked voltage time courses show that EPSPs are a composition of many synaptic mini-EPSPs released with a particular time distribution. Decay phase is similar between the bilateral responses dictated by "effective" membrane time constant (combination of active currents) and integration properties of bipolar dendrites. (C) Top row: slopes versus halfwidth for PSPs evoked from contralateral and ipsilateral stimulations. Ipsilateral responses are steeper than contralateral, with similar halfwidth for both responses. Passive propagation of EPSP through asymmetric dendrites is not enough to explain the difference on asymmetric responses recorded at the soma compartment due to the similarity in halfwidths. Normalizing the halfwidths and slopes by the corresponding individual PSP amplitudes show consistent results supporting the fundamental observation that the bilateral asymmetry is intrinsic in the neurons independently from the trials and response amplitude. Bottom row: same as the top row but now glycinergic inhibition is blocked. Note: EPSP shapes are similar to the ones obtained from the model when we simulate the synaptic excitatory conductance as population of inputs with different jitter for each bilateral input (see also Figure 3 and Figure S4). In vivo EPSP slopes could be smaller than the ones recorded in our experiments due to the fact that in our preparation there is a high degree of synchronicity due to the simultaneous stimulation of the VCN bundle. Larger ipsilateral response will strongly support our results. For simplicity and taking a conservative position we will use for the modeling equal amount of conductance between bilateral inputs. Only for some schematics will we use the same amplitude for bilateral inputs.

Found at: doi:10.1371/journal.pbio.1000406.s002 (0.85 MB EPS)

**Figure S3 Increase in slope due to fast and slow (extreme values) inhibitory conductance (from our parameter study this effect is seen if  $0.2 \text{ (ms)} < \delta$  for  $\tau_{inh} = 0.1 \text{ (ms)}$  and  $0.75 \text{ (ms)} < \delta$  for  $\tau_{inh} = 1.0 \text{ (ms)}$ ).** EPSPs with a shallower slope are more affected by synaptic inhibition for a large range of inhibitory synaptic input's time scale. Therefore, for the time scale of our recorded contralateral inputs, they will be more affected by inhibitory conductance than their ipsilateral counterparts. (A) Time courses for PSPs in the case of fast and slow synaptic inhibition ( $\delta$  is the time that inhibition leads excitation). (B) Simulation (using the neuron model, see Methods) of PSP (EPSP + IPSP) generated with synaptic fast IPSPs having time scale of  $\tau_{inh} = 0.1 \text{ ms}$  and advanced with respect to the EPSPs by  $\delta = 0.2 \text{ ms}$ . Two different EPSPs examples:  $0.15 \text{ ms}$  (red, for ipsilateral input) or  $0.25 \text{ ms}$  (blue, for contralateral input). (C) Simulation with synaptic IPSPs with time scale of  $\tau_{inh} = 1.0 \text{ ms}$  and advanced with respect to the EPSPs by  $\delta = 1.0 \text{ ms}$  (point of full activation). Two cases:  $\tau_{exc} = 0.15 \text{ ms}$  (example for ipsilateral input, red),  $0.25 \text{ ms}$  (example for contralateral input, blue). For an equivalent change in synaptic inhibitory conductance ( $\Delta G_{inh}$ ), the slope of the shallower EPSP displayed a greater change (arrow)

## References

- Grothe B (2003) New roles for synaptic inhibition in sound localization. *Nat Rev Neurosci* 4: 540–550.
- Joris P, Yin TC (2007) A matter of time: internal delays in binaural processing. *Trends Neurosci* 30: 70–78.
- Jeffress LA (1948) A place theory of sound localization. *J Comp Physiol Psychol* 41: 35–39.
- Young SR, Rubel EW (1983) Frequency specific projections of individual neurons in chick brainstem auditory nuclei. *J Neurosci* 3: 1373–1378.

than steeper EPSPs. If contralateral EPSPs have shallower rising slopes, then they are more affected by inhibition than ipsilateral EPSPs (Note: the range of total inhibitory conductance is the same in (B) and (C), since  $G_{inh,MAX}$  is proportional to  $\tau_{inh}$ ).

Found at: doi:10.1371/journal.pbio.1000406.s003 (0.60 MB EPS)

**Figure S4 Composite EPSPs and IPSPs for an input train (500 Hz) using an idealized auditory nerve fiber model (sinusoidally modulated Poisson rate for mini-PSG times), less realistic than (Carney 1993)[18].** (A) Raster plots with event times for ipsilateral excitatory inputs (red), contralateral excitatory inputs (blue), and contralateral inhibitory inputs (green). Superposition of composite PSGs for these three cases. Mini-EPSPs are alpha functions with time constant of  $0.1 \text{ ms}$ , and mini-IPSPs are alpha functions of  $0.4 \text{ ms}$  time const. The difference in vector strength (degree of synchrony) between the events dictates the shape of the composite EPSPs and IPSPs. Similar composite IPSPs can be generated with mini-IPSPs made of alpha functions of  $0.1 \text{ ms}$  time constant and lower vector strength ( $R = 0.48$ ). (B) Composite PSCs corresponding to the PSGs from the final cycle of the time series in (A). EPSCs obtained with higher vector strength have steeper rising slope and shorter halfwidth (red, ipsilateral inputs; blue, contralateral inputs). IPSCs look similar to inhibitory conductance time course, because the temporal summation reached a steady state dynamic. (C) PSPs for the last cycle in (A) for the three input cases. Superimposed with a thick line is the average time course for EPSPs and IPSPs. Rising slopes are steeper when vector strength is larger (ipsilateral EPSP has steeper slope). (D) Average over 25 cycles of composite PSGs for the three different inputs. In the three cases a function (dashed) was fitted to the average PSG. Alpha function is the simplest description of PSGs (long dashes); it fits the rising phase but not the falling phase. Composite EPSPs were fitted with a functional form that is proportional to  $(1 - (\exp(-(t-t_0)/\tau_{rise}))) \cdot 3 \cdot (\exp(-(t-t_0)/\tau_{decay}))$ . Ipsilateral inputs (red):  $\tau_{rise} = 2.5$ ,  $\tau_{decay} = 0.14$ . Contralateral inputs (blue):  $\tau_{rise} = 2.8$ ,  $\tau_{decay} = 0.18$ . For the alpha function fits, for ipsilateral inputs (red):  $\tau = 0.48$ ; for contralateral inputs (blue):  $\tau = 0.69$ . In the case of inhibition the best fitting was obtained with a periodic function  $(a \cdot \sin((t-t_0)/n) + b)$ , due to the time constant of the individual components and the temporal summation generated at this frequency.

Found at: doi:10.1371/journal.pbio.1000406.s004 (1.83 MB EPS)

## Acknowledgments

We thank Jaime de la Rocha, Max Schiff, Anne Takesian, Sach Sokol, and Alex Reyes for fruitful discussions and comments on an earlier version of this manuscript.

## Author Contributions

The author(s) have made the following declarations about their contributions: Conceived and designed the experiments: PEJ. Performed the experiments: PEJ. Analyzed the data: PEJ. Contributed reagents/materials/analysis tools and trained PEJ in doing the experiments: GS VCK. Wrote the paper: PEJ. Direct the research and manuscript preparation: DHS JR.

8. Beckius GE, Batra R, Oliver DL (1999) Axons from anteroventral cochlear nucleus that terminate in medial superior olive of cat: observations related to delay lines. *J Neurosci* 19: 3146–3161.
9. Yin TCT, Chan JK (1990) Interaural time sensitivity in medial superior olive in cat. *J Neurophysiol* 64: 465–488.
10. Spitzer MW, Semple MN (1995) Neurons sensitive to interaural phase disparity in gerbil superior olive: diverse monaural and temporal response properties. *J Neurophysiol* 73: 1668–1690.
11. Brand A, Behrend O, Marquardt T, McAlpine D, Grothe B (2002) Precise inhibition is essential for microsecond interaural time difference coding. *Nature* 417: 543–547.
12. Shackleton TM, Skottun BC, Arnott RH, Palmer AR (2003) Interaural time difference discrimination thresholds for single neurons in the inferior colliculus of guinea pigs. *J Neurosci* 23: 716–724.
13. Harper NS, MacAlpine D (2004) Optimal neural population coding of an auditory spatial cue. *Nature* 430: 682–686.
14. Pecka M, Brand A, Behrend O, Grothe B (2008) Interaural time difference processing in the mammalian medial superior olive: the role of glycinergic inhibition. *J Neurosci* 28: 6914–6925.
15. Joris PX, Yin TC (1998) Envelope coding in the lateral superior olive. III. Comparison with afferent pathways. *J Neurophysiol* 79: 253–269.
16. Heffner RS, Heffner HE (1988) Sound localization and use of binaural cues by the gerbil (*Meriones unguiculatus*). *Behav Neurosci* 102: 422–428.
17. Brughera AR, Stutman ER, Carney LH, Colburn HS (1996) A model with excitation and inhibition for cells in the medial superior olive. *Aud Neurosci* 2: 219–233.
18. Carney LH (1993) A model for the responses of low-frequency auditory-nerve fibers in cat. *J Acoust Soc Am* 93: 401–417.
19. McGinley MJ, Oertel D (2006) Rate thresholds determine the precision of temporal integration in principal cells of the ventral cochlear nucleus. *Hear Research* 216–217: 52–63.
20. Scott LL, Mathews PJ, Golding NL (2005) Posthearing developmental refinement of temporal processing in principal neurons of the medial superior olive. *J Neurosci* 25: 7887–7895.
21. Scott LL, Hage TA, Golding NL (2007) Weak action potential backpropagation is associated with high-frequency axonal firing capability in principal neurons of the gerbil medial superior olive. *J Physiol* 583: 647–661.
22. Svirskis G, Kotak V, Sanes DH, Rinzel J (2002) Enhancement of signal-to-noise ratio and phase locking for small inputs by a low-threshold outward current in auditory neurons. *J Neurosci* 22: 11019–11025.
23. Svirskis G, Kotak V, Sanes DH, Rinzel J (2004) Sodium along with low-threshold potassium currents enhance coincidence detection of subthreshold noisy signals in MSO neurons. *J Neurophysiol* 91: 2465–2473.
24. Goldberg EM, Clark BD, Zhaga E, Nahmani M, Erisir A, et al. (2008) K<sup>+</sup> channels at the axon initial segment dampen near-threshold excitability of neocortical fast-spiking GABAergic interneurons. *Neuron* 58: 387–400.
25. Wilent WB, Contreras D (2005) Dynamics of excitation and inhibition underlying stimulus selectivity in rat somatosensory cortex. *Nat Neurosci* 8: 1364–1370.
26. Chadderton P, Agapiou JP, McAlpine D, Margrie TW (2009) The synaptic representation of sound source location in auditory cortex. *J Neurosci* 29: 14127–14135.
27. Seidl AH, Rubel EW, Harris DM (2010) Mechanisms for adjusting interaural time differences to achieve binaural coincidence detection. *J Neurosci* 30: 70–80.
28. Ferragamo MJ, Oertel D (2002) Octopus cells of the mammalian ventral cochlear nucleus sense the rate of depolarization. *J Neurophysiol* 87: 2262–2270.
29. Agmon-Snir H, Carr CE, Rinzel J (1998) The role of dendrites in auditory coincidence detection. *Nature* 393: 207–208.
30. Rall W, et al. (1992) Matching dendritic neuron models to experimental data. *Physiol Rev* 72: 159–186.
31. Spruston N, Jaffe DB, Williams SH, Johnston D (1993) Voltage- and space-clamp errors associated with the measurement of electrotonically remote synaptic events. *J Neurophys* 70: 781–208.
32. Mathews PJ, Jercog PE, Rinzel J, Scott LL, Golding LL (2010) Control of submillisecond synaptic timing in binaural coincidence detectors by K<sub>v1</sub> channels. *Nat Neurosci* online: DOI: 10.1038/nn.2530.
33. Oviedo H, Reyes AD (2002) Boosting of neuronal firing evoked with asynchronous and synchronous inputs to the dendrite. *Nat Neurosci* 5: 261–266.
34. Magnusson AK, Kapfer C, Grothe B, Koch U (2005) Maturation of glycinergic inhibition in the gerbil medial superior olive after hearing onset. *J Physiol* 568: 497–512.
35. Chirila FV, Rowland KC, Thompson JM, Spirou GA (2007) Development of gerbil medial superior olive: integration of temporally delayed excitation and inhibition at physiological temperature. *J Physiol* 584: 167–190.
36. Rothman JS, Manis PB (2003) Kinetic analyses of three distinct potassium conductances in ventral cochlear nucleus neurons. *J Neurophysiol* 89: 3083–3096.